FAU-Type Zeolite Nanocasted Carbon Replicas for CO2 Adsorption and Hydrogen Purification

ARTICLE *in* ENERGY & FUELS · MAY 2010

Impact Factor: 2.79 · DOI: 10.1021/ef100011q

5 AUTHORS, INCLUDING:

Julien Parmentier
Université de Haute-Alsace
95 PUBLICATIONS **1,780** CITATIONS
SEE PROFILE

Gerhard Pirngruber
IFP Energies nouvelles
101 PUBLICATIONS **2,208** CITATIONS
SEE PROFILE

Energy Fuels **XXXX,** *XXX,* 000–000 · DOI:10.1021/ef100011q

energy&fuels
article

FAU-Type Zeolite Nanocasted Carbon Replicas for CO_2 Adsorption and Hydrogen Purification

Claire Ducrot-Boisgontier,[†] Julien Parmentier,*[,†] Azzam Faour,[†,‡] Joël Patarin,[†] and Gerhard D. Pirngruber[‡]

[†]*Institut de Science des Matériaux de Mulhouse, LRC CNRS 7228, Université de Haute Alsace, 15 rue Jean Starcky, BP 2488, 68057 Mulhouse Cedex, France, and* [‡]*Catalysis and Separation Division, IFP, BP3, F-69360 Solaize, France*

Received January 19, 2010. Revised Manuscript Received May 10, 2010

Microporous ordered carbon have been synthesized by the nanocasting process from zeolite Y using acetylene and furfuryl alcohol as carbon precursors. If the proper synthesis conditions are chosen, these materials retain the long-range order of the zeolite mold. The resulting carbons possess a large surface area ($\geq$2200 m^2/g), a high microporosity ($\geq$1.0 cm^3/g), and a controlled pore size distribution, which was tailored by the wall thickness of the zeolite template. Because of their high micropore volume, the carbon replicas of zeolite Y are attractive adsorbent materials and might be used to replace conventional activated carbons as adsorbents in pressure swing adsorption processes (PSAs) for H_2 purification. In the present contribution, we evaluate the adsorption capacity of the carbon replicas in a H_2-PSA based on their single-component adsorption isotherms of CO_2, CH_4, and N_2 measured at room temperature. The ideal adsorbed solution theory (IAST) was used to predict the co-adsorption of $CO_2/CH_4/N_2$ gas mixtures and to evaluate the working capacity of the materials under typical operating conditions of a H_2-PSA process. The comparison of the working capacities shows that the carbon replicas largely outperform conventional activated carbons while having comparable CO_2/CH_4 and CO_2/N_2 selectivity.

Introduction

Activated carbon materials are widely used as adsorbents in various separation and purification processes. One of the most important applications is the purification of hydrogen from synthesis gas composed of H_2, CO_2, CH_4, CO, N_2, etc. The impurities are separated from H_2 by pressure swing adsorption (PSA). Current H_2-PSA processes use a multi-layer adsorbent bed, which contains in a first layer a drying agent (silica gel or alumina), a second layer of activated carbon, which adsorbs mainly CO_2 and heavy hydrocarbons (if present), and finally, a layer of zeolite X or A, which traps the weakly adsorbed impurities from the gas mixture (CH_4, CO, N_2, etc.). In view of the rising demand for hydrogen, there is a need to increase the efficiency of the H_2-PSA process. In particular, there is room for improvement of the adsorption properties of the activated carbons used for H_2 purification, in terms of their working capacity. Conventional activated carbons are prepared from natural precursors (coal, peat, wood, nutshells, olive stones, etc.). Their porosity is generated by physical or chemical activation procedures. These methods lead to a non-ordered porosity and generally a rather large pore size distribution (PSD).

Nowadays, various methods are known to prepare synthetic carbon materials that allow for a much better control of the porosity. One of the most interesting examples is the synthesis of ordered porous carbon materials by nanocasting.[1−3] These materials have a narrow micropore size distribution, a large pore volume with hardly any meso- or macroporosity, and a high specific surface area comparable to activated carbons. Therefore, these materials appear as very interesting candidates for the adsorption of CO_2 in PSA processes. Their high surface areas are obtained without any activation process, and therefore, these materials do not exhibit the peculiar surface functionalities generated by the different activating agents. The nanocasting process creates an inverse replication of a porous template (e.g., zeolite or ordered mesoporous silica) by infiltrating its porosity with organic material, which is subsequently converted to carbon. The removal of the template leads to a negative carbon replica, whose porous characteristics are derived from the templated structure (e.g., size and shape of the porous network) and the nature of the carbon precursor. If meso-structured or crystalline porous templates are used, a nano-ordered porous structure can be obtained with a porosity corresponding to the template wall thickness. Zeolites are particularly interesting molds because they lead to microporous carbon materials with narrow micropore size distributions, large pore volumes, and high specific surface areas compared to activated carbons.[4]

The zeolite faujasite Y (FAU-type structure) is most frequently employed as a template.[1,2,5] Its three-dimensional porosity is particularly well-suited for nanocasting, and the material is fairly stable and has the advantage of being commercially available. Faujasite Y displays cubic symmetry (space group of $Fd\bar{3}m$), and its framework is formed by interconnected cages of ~1.2 nm in diameter (if the space occupied by the extra framework cations is taken into account, the free diameter of the cages is reduced to ~1.0 nm). High-quality carbon replicas of faujasite Y show an X-ray diffraction peak at around $2\theta = 6°$ (Cu Kα1), which indicates that the structural periodicity of the (111) planes of zeolite Y has been maintained. Their pore volume and

*To whom correspondence should be addressed. E-mail: julien.parmentier@uha.fr.

(1) Kyotani, T. *Bull. Chem. Soc. Jpn.* **2006**, *79*, 1322–1337.
(2) Lee, J.; Kim, J.; Hyeon, T. *Adv. Mater.* **2006**, *18*, 2073–2094.
(3) Gaslain, F. O. M.; Parmentier, J.; Valtchev, V. P.; Patarin, J. *Chem. Commun.* **2006**, 991–993.
(4) Barata-Rodrigues, P. M.; Mays, T. J.; Moggridge, G. D. *Carbon* **2003**, *41*, 2231–2246.
(5) Ma, Z.; Kyotani, T.; Tomita, A. *Carbon* **2002**, *40*, 2367–2374.

specific surface area are high (>1 cm^3/g and >2000 m^2/g, respectively) and the pore volume is almost entirely microporous. High-quality carbon replicas are usually obtained when a two-step infiltration is performed.[5,6] The first step is the impregnation of zeolite with furfuryl alcohol, which is polymerized. To increase the loading of the pores with organic material, chemical vapor deposition (CVD) of propylene is then employed in a second step. This two-step procedure seems to be essential to obtain a microporous carbon, but it is long and laborious. Hou et al.[7] showed that it was possible to obtain a microporous carbon replica using only acetylene (deposited by CVD) as the carbon precursor.

These carbon replicas have high potential in various applications. They have shown relatively good hydrogen storage capacity (~2% weight at 77 K and 1 bar)[8−15] and have also been proposed for CH_4 storage. Because of their high micropore volumes, the carbon replica could also be very interesting adsorbents for PSA processes, in particular for the adsorption of CO_2 in H_2-PSAs. The performance of a CO_2 adsorbent in a PSA process mainly depends upon the working capacity of CO_2 (the difference in the adsorption capacity between the adsorption and desorption steps), being in co-adsorption with the other components of the feed, which are mainly CH_4, CO, and N_2. To estimate the working capacity, we have measured at room temperature the adsorption isotherms of the main components present in synthesis gas, i.e., H_2, CO_2, CH_4, and N_2, on carbon replicas of faujasite Y. The behavior in co-adsorption of $H_2/CO_2/CH_4/N_2$ mixtures was evaluated using the ideal adsorbed solution theory (IAST), and the data were compared to commercial activated carbons.

Experimental Section

The microporous carbon materials were prepared using zeolite Y [Na form, Si/Al (molar ratio) = 2.7, Aldrich] as the template. We attempted to fill the zeolite nanopores with carbon by the following two methods.

Method 1:[7] Acetylene CVD (5% in argon by volume) was performed over dried zeolite Y in powder form (placed in the quartz boat) at 873 K for 4 h. A portion of this zeolite/carbon composite was subjected to a secondary CVD treatment using acetylene at 973 K for 1 h.

Method 2:[5] The zeolite pores were first filled with furfuryl alcohol (FA) by impregnation. The mixture of zeolite and FA was stirred at room temperature for 24 h, filtered, and washed with mesitylene to remove the excess of FA on the external surface of the zeolite powder. The FA was polymerized inside the zeolite channels by heating the powder at 353 K for 24 h and then at 423 K for 8 h in a nitrogen flow. The polyfurfurlyalcohol (PFA)/zeolite composite was then placed in a quartz boat and subjected to acetylene CVD under argon flow at 873 K for 4 h and 973 K for 1 h or at 923 K for 5 h.

Finally, a heat treatment at 1173 K for 4 h under argon flow was performed on all zeolite/carbon composites to improve the structural organization of the carbon replicas as evidenced by Ma et al.[6] The resulting carbon frameworks were liberated by etching the zeolite framework with an excess amount of 40 wt % aqueous HF solution at room temperature for 24 h. The resulting black powder was then filtered, washed with distilled water, and refluxed with an excess of HCl (36 wt %) for 4 h to ensure complete dissolution of the inorganic template and subsequent byproducts. The carbon powders were filtered and washed with distilled water. Hereafter, the samples were named [carbon precursor: Ac, acetylene; FA, furfuryl alcohol]-[temperature of CVD in kelvin]-[time of CVD in hours]. For instance, FA+Ac-873/973-4/1 means FA infiltration followed by CVD of acetylene at 873 K for 4 h and CVD of acetylene at 973 K for 1 h. The amount of carbon present into the zeolite/carbon composites were determined by thermogravimetric analysis (Seteram Labsys in air) from the weight loss by oxidation of the carbonaceous part of the composite in the range of 300−800 °C.

Two commercial activated carbons were tested for a comparison to the carbon replicas, i.e., AC35 and BG-ENO (from CECA Company). The physically activated carbon AC35 is mainly microporous, whereas the chemically activated carbon BG-ENO has a broader PSD with super-micropores and mesopores. Moreover, because of the use of different activating agents, surface chemical functional groups are expected to be present.[16,17]

The structure of the nanocasted carbons was examined by X-ray diffraction (XRD). The powder XRD pattern was performed using a STADI-P STOE diffractometer with Cu Kα1 radiation ($\lambda = 1.5406$ Å) (40 kV, 30 mA).

Textural properties were determined via a nitrogen sorption isotherm at 77 K (ASAP 2420, Micromeretics). Before the experiments, the samples were outgassed under vacuum at 363 K for 1 h and at 573 K overnight. The Brunauer−Emmett−Teller (BET) surface area of all of the carbons was determined using the data in the relative pressure range of 0.01−0.05.[18] The micropore volume was calculated from the Dubinin−Radushkevich equation. The mesopore volume was determined by subtracting the micropore volume from the volume of N_2 adsorbed at a relative pressure of 0.95. The PSDs of carbon replicas were given with the non-local density functional theory (NLDFT) method for cylindrical pores using the software provided by Micromeritics [models N_2-Tarazona NLDFT, electrostatic force (esf) = 30.0 K][19] because the micropore morphology, related to the zeolite structure, is better described by (interconnected) cylindrical pores rather than infinite slit-like pores. For activated carbons, the PSD is determined using the density functional theory (DFT) model for slit-like pores (N_2-DFT model).

Thermogravimetric analysis (TGA) was performed using Seteram Labsys with a heating rate of 5 K/min under static air. Carbon fractions in the carbon/zeolite composites were determined from the weight loss by oxidation of the carbonaceous part of the composite in the range of 573−1073 K.

The gas (CO_2, CH_4, N_2, and H_2) adsorption properties of the carbon were evaluated at 298 K by gravimetry using a magnetic suspension balance (Rubotherm). The carbon samples were degassed under vacuum at 423 K for 2 h, and then the adsorption/desorption isotherms were recorded at room temperature in the range of 0.2−30 bar. The desorption isotherms were always superposed with the adsorption isotherms; i.e., the adsorption was perfectly reversible. The Rubotherm balance measures an

(6) Ma, Z.; Kyotani, T.; Liu, Z.; Terasaki, O.; Tomita, A. *Chem. Mater*. **2001**, *13*, 4413–4415.
(7) Hou, P.-X.; Yamazaki, T.; Orikasa, H.; Kyotani, T. *Carbon* **2005**, *43*, 2624–2627.
(8) Armandi, M.; Bonelli, B.; Bottero, I.; Arean, C. O.; Garrone, E. *Microporous Mesoporous Mater*. **2007**, *103*, 150–157.
(9) Chen, L.; Singh, R. K.; Webley, P. *Microporous Mesoporous Mater*. **2007**, *102*, 159–170.
(10) Roussel, T.; Didion, A.; Pellenq, R. J. M.; Gadiou, R.; Bichara, C.; Vix-Guterl, C. *J. Phys. Chem. C* **2007**, *111*, 15863–15876.
(11) Yang, Z. X.; Xia, Y. D.; Sun, X. Z.; Mokaya, R. *J. Phys. Chem. B* **2006**, *110*, 18424–18431.
(12) Pacula, A.; Mokaya, R. *J. Phys. Chem. C* **2008**, *112*, 2764–2769.
(13) Yang, Z. X.; Xia, Y. D.; Mokaya, R. *J. Am. Chem. Soc*. **2007**, *129*, 1673–1679.
(14) Guan, C.; Wang, K.; Yang, C.; Zhao, X. S. *Microporous Mesoporous Mater*. **2009**, *118*, 503–507.
(15) Guan, C.; Zhang, X.; Wang, K.; Yang, C. *Sep. Purif. Technol*. **2009**, *66*, 565–569.
(16) Puziy, A. M.; Poddubnaya, O. I.; Martinez-Alonso, A.; Suarez-Garcia, F.; Tascon, J. M. D. *Carbon* **2002**, *40*, 1493–1505.
(17) Molina-Sabio, M.; Gonzalez, M. T.; Rodriguez-Reinoso, F.; Sepúlveda-Escribano, A. *Carbon* **1996**, *34*, 505–509.
(18) Kaneko, K.; Ishii, C. *Colloids Surf*. **1992**, *67*, 203–212.
(19) Tarazona, P.; Marconi, U. M. B.; Evans, R. *Mol. Phys*. **1987**, *60*, 573–595.

apparent mass that has to be corrected for the buoyancy of the sample and the sample holder. For this purpose, the volume of the sample and sample holder was therefore determined by measuring the buoyancy effect with a non-adsorbing gas, i.e., He.

The pure isotherms were fitted by a Langmuir equation (eq 1) to obtain the values of Henry's law constant (K_{Henry}) by the relation $K_{Henry} = q_s b$, where q_s is the adsorbed quantity at saturation, b is the adsorption constant, and P is the pressure.

$$q = \frac{q_s b P}{1 + bP} \quad (1)$$

In a second step, the adsorption isotherms of the pure component were fitted by a Toth equation (eq 2), and these fits were used to calculate mixture selectivities according to ideal adsorbed solution theory, with m being a constant that allows us to take into account the heterogeneity of the adsorption sites. The other parameters have the same meaning as in the Langmuir equation.

$$q = \frac{q_s b P}{[1+(bP)^m]^{1/m}} \quad (2)$$

The IAST model allows for the prediction of the co-adsorption of gas mixtures based on the pure component adsorption isotherms.[20] It assumes that the adsorbed phase behaves like an ideal solution (with the activity coefficient of each component being equal to unity) and is therefore analogous to Raoult's law for vapor−liquid equilibria. It has been shown that, among a number of different co-adsorption models, IAS gives the most precise prediction of the co-adsorption of CO_2−CH_4 mixtures on activated carbons.[21] We have therefore used IAS to predict the selectivities α in co-adsorption of 50:50 mixtures of CO_2/CH_4 and CO_2/N_2. The value of the selectivity α was calculated from eq 3, where x_{CO_2} and y_{CO_2} are the molar fractions in the adsorbed and gas phases, respectively.

$$\alpha = \frac{\dfrac{x_{CO_2}}{y_{CO_2}}}{\dfrac{(1-x_{CO_2})}{(1-y_{CO_2})}} \quad (3)$$

At low pressure, the selectivity calculated by IAS can be compared to the ratio of Henry's law constants $K_{Henry\ i}/K_{Henry\ j}$ of the pure components.

Results

The structural ordering of the carbon replicas was evaluated by powder XRD (Figure 1). The carbon replicas Ac-873/973-4/1, FA+Ac-923-5, and FA+Ac-873/973-4/1 display one diffraction peak at around $2\theta = 6.5°$. This peak has a d spacing similar to the (111) planes of zeolite Y and indicates that the carbon replicas are well-ordered and have the same symmetry as the zeolite mold. The degree of organization is related to the peak intensity and decreases in the sequence FA+Ac-873/973-4/1 > Ac-873/973-4/1 > AF+Ac-923-5. The absence of diffraction peaks typical for graphene stacking (expected at around $2\theta = 25°$) reveals the non-graphitic nature of the carbon replicas, which have a tubular or flake structure as described in the literature.[10,22] Moreover, it proves that the amount of graphitic carbon deposits on the external surface is negligible.

The N_2 adsorption isotherms (77 K) of carbon replicas and activated carbon are shown in Figure 2. The isotherms of carbon replicas and AC35 material are mainly of type Ib, according to the International Union of Pure and Applied

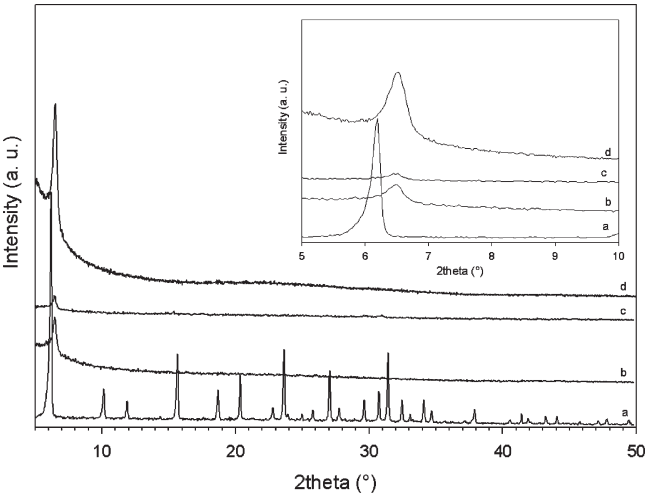

Figure 1. XRD patterns (Cu Kα1 radiation) of (a) zeolite Y (FAU-type structure) and the carbon replicas (b) Ac-873/973-4/1, (c) FA+Ac-923-5, and (d) FA+Ac-873/973-4/1. (Inset) Zoom in the range of 5−10° (2θ).

Chemistry (IUPAC) classification,[23] with a high nitrogen uptake in the low relative pressure domain ($P/P_0 = 0-0.01$). This behavior reveals the super-microporous character of these carbon materials (1.0 nm < pore diameter < 2.0 nm). The isotherm of activated carbon BG-ENO is a mixture of types I and IV, indicating the presence of both micro- and mesopores. The specific surface area and pore volume values are reported in Table 1.

The carbon replicas present a large specific surface area (2176−3213 m^2/g) and a high pore volume (1.1−1.6 cm^3/g). Most of the pore volume is due to micropores (0.9−1.4 cm^3/g). Interestingly, there is a correlation between the surface area and pore volume and the intensity of the XRD peak at $2\theta = 6°$. The material FA+Ac-873/973-4/1 has the most intense XRD peaks and also displays the highest specific surface area (3213 m^2/g) and pore volume (1.6 cm^3/g). The amount of carbon (around 25 wt %; Table 1) deposited in the corresponding composite material is also the highest. On the other hand, FA-Ac-923-5 has the lowest carbon content in the precursor, the lowest surface area and pore volume, and the weakest XRD peak. A good infiltration of NaY with carbon precursors seems to be important for the quality of the replication. Previous studies[5,24] have shown that an initial infiltration with FA followed by CVD of acetylene or propylene improves the quality of replication compared to direct use of CVD. Nevertheless, it appears that the temperature profile chosen for the CVD step is very important. A low-temperature CVD process (873 K) probably allows for a longer mean free path of the reacting species within the porous template and, therefore, a more homogeneous filling of the host material. The secondary treatment at 973 K associated with a higher carbon deposition amount completes the filling of the mold and thereby avoids the collapse of the carbon nanostructured framework. On the opposite side, the fast deposition at 973 K also promotes the pore blockage from the outer surface, resulting to an incomplete filling of the mold, as evidenced by the broad PSD around 1.8 nm (see PSD curves in

(20) Myers, A. L.; Prausnitz, J. M. *AIChE J.* **1965**, *11*, 121–127.
(21) Ritter, J. A.; Yang, R. T. *Ind. Eng. Chem. Res.* **1987**, *26*, 1679–1686.
(22) Nishihara, H.; Yang, Q. H.; Hou, P. X.; Unno, M.; Yamauchi, S.; Saito, R.; Paredes, J. I.; Martinez-Alonso, A.; Tascon, J. M. D.; Sato, Y.; Terauchi, M.; Kyotani, T. *Carbon* **2009**, *47*, 1220–1230.
(23) Sing, K. S. W.; Everett, D. H.; Haul, R. A. W.; Moscou, L.; Pierotti, R. A.; Rouquerol, J.; Siemieniewska, T. *Pure Appl. Chem.* **1985**, *57*, 603–619.
(24) Ducrot-Boisgontier, C.; Parmentier, J.; Patarin, J. *Microporous Mesoporous Mater.* **2009**, *126*, 101–106.

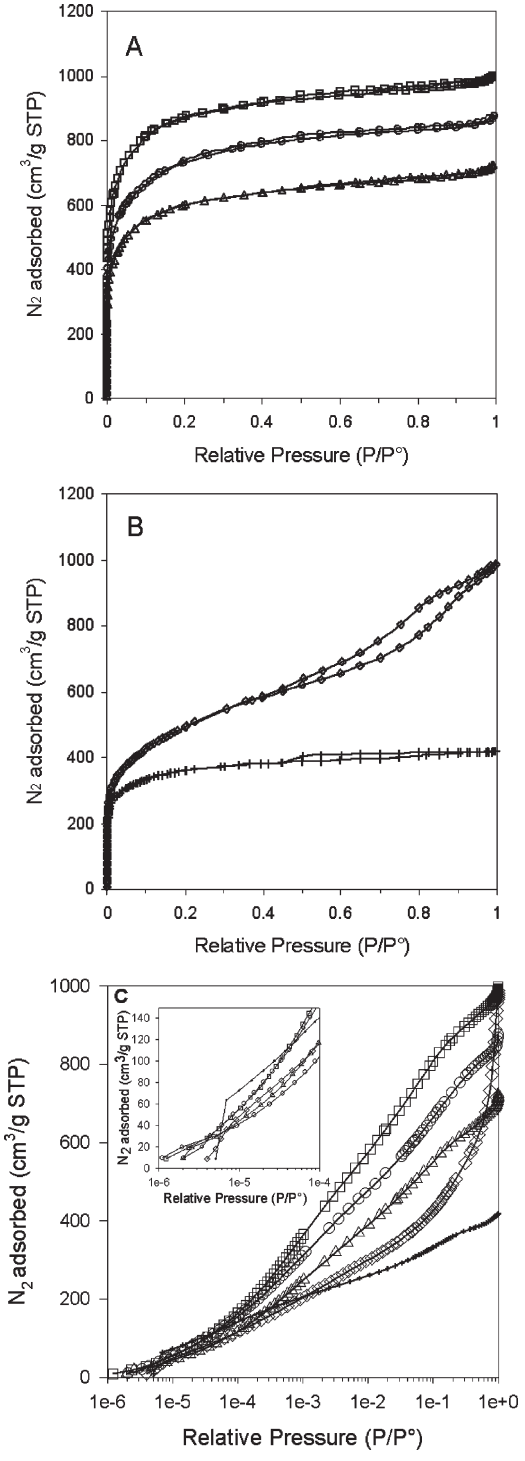

Figure 2. N_2 adsorption/desorption isotherms (77 K) of (A) carbon replicas prepared by (○) Ac-873/973-4/1, (△) FA+Ac-923-5, (□) and FA+Ac-873/973-4/1 and (B) activated carbons (+) AC35 and (◇) BG-ENO. (C) N_2 adsorption/desorption isotherms (77 K) in $P/P_0 = 10^{-6} \rightarrow 1.0$. (Inset) Zoom in the range from 10^{-6} to 10^{-4}.

Figure 3). Nevertheless, this two-step CVD treatment appears to optimize the ordering of the structure, because even the Ac-873/973-4/1 sample (no FA used) is better ordered than the FA+Ac-923-5 sample (CVD in one step). The CVD temperature of 923 K for the latter sample is probably too high to lead to a homogeneous and rigid carbon framework.

The PSD determined by the NLDFT method (Figure 3A) shows that the porosity of the carbon replicas consists of three types of pores with a mean diameter of 0.7, 1.0, and 1.8 nm. The first peak in the PSD at 0.7 nm is attributed to adsorption in ultra-micropores or on localized sites, for example, defects inside the carbon walls. The second maximum (around 1.0 nm) can be attributed to the replication of the zeolite mold. Indeed, the sodalite cages of faujasite Y have a diameter around 1.0 nm, and their etching yields an ordered pore network with a pore diameter close to 1 nm and with a periodicity of 1.34 nm, as evidenced by the presence of the XRD peak. This pore size has also been suggested by other studies based on atomic simulations.[10] The third maximum at 1.8 nm arises from the incomplete filling of the zeolite template. The minima in the PSD at 1.5 nm may be an artifact of the DFT model related to the cylindrical pore shape chosen for those materials.

The commercial activated carbon materials have much lower surface areas than the carbon replicas (1310−1653 m^2/g). The carbon AC35 has a low pore volume (0.6 cm^3/g) composed mainly of micropores (0.5 cm^3/g). Its PSD (determined using the DFT method for slit-like pores) is quite similar to those of the carbon replicas (Figure 3B). There are three peaks, at 0.8, 1.5, and 2.5 nm; i.e., the pore size is shifted to slightly higher values than in the carbon replicas. The zoom of the N_2 isotherm at 77 K at very low pressures shows that the carbon AC35 has the largest amount of very narrow micropores (pores that are filled below $P/P_0 = 5 \times 10^{-5}$ at 77 K; see Figure 2C). The minimum of the PSD observed at 1.0 nm is a well-know DFT calculation artifact, as explained in ref 25, when slit-pore geometry is used for activated carbon materials. Therefore, caution should be taken in the comparison of cumulative pore volume distribution (see Figure S1 in the Supporting Information) because of the possible presence of artifacts around 1.0 and 1.5 nm for activated and replicated carbons, respectively, where different pore geometry have been considered. The carbon BG-ENO displays a large pore volume (1.4 cm^3/g), but the contribution of mesopores is not negligible (0.8 cm^3/g). Its PSD has maxima at 0.8, 1.5, 3, and 10 nm, and the porosity spreads up to 40 nm. In terms of cumulative pore volume, it overtakes AC35 at a pore size of 1.5 nm and FA+Ac-923-5 at a pore size of 10 nm (see Figure S1 in the Supporting Information).

The CO_2, N_2, and CH_4 adsorption isotherms at 298 K of carbon replicas and activated carbons are given in Figures 4−6.

The adsorption capacity of samples decreases in the sequence $CO_2 > CH_4 > N_2 > H_2$ (see Figure 7). This sequence is generally observed for activated carbons and follows the boiling temperatures of these molecules (195, 112, and 77 K at atmospheric pressure, respectively). Among the carbon replicas, the adsorbed amount follows the quality of the nanocasting, i.e., in the order FA+Ac-873/973-4/1 > Ac-873/973-4/1 > FA+Ac-923-5. There is always a clear difference between the sorption capacity of FA+Ac-873/973-4/1 and FA+Ac-923-5, which does not have a well-ordered porosity. This result underlines the importance of producing a replication of high quality. It assures a high surface area and pore volume and, hence, leads to a high adsorption capacity. Only the N_2 isotherms at 298 K do not strictly follow the order of surface areas and pore volumes; we find only little difference in the N_2 adsorption capacity of the two samples FA-Ac-873/973-4/1 and Ac-873/973-4/1 (Figure 5).

With the exception of the low-pressure range of the isotherms (< 2 bar), the carbon replicas, including the less

(25) Ravikovitch, P. I.; Vishnyakov, A.; Russo, R.; Neimark, A. V. *Langmuir* **2000**, *16*, 2311–2320.

Table 1. Carbon Amounts in Carbon/Zeolite Composites, Equivalent Surface Areas, Pore Volumes, and Densities of the Carbon Replicas and Activated Carbons

	carbon amount (wt %)[a]	equivalent surface area BET (m^2/g)[b]	pore volume (cm^3/g) V_t[c]	V_{micro}[d]	V_{meso}[e]	skeletal density (g/cm^3)[f]	apparent density (g/cm^3)[g]
Ac-873/973-4/1	20	2609	1.3	1.2	0.1	2.3	0.57
FA+Ac-923-5	19	2176	1.1	0.9	0.2	2.3	0.67
FA+Ac-873/973-4/1	25	3213	1.6	1.4	0.2	2.0	0.49
AC35		1310	0.6	0.5	0.1	1.8	0.92
BG-ENO		1653	1.4	0.8	0.6	1.7	0.50

[a] Determined by TGA data from the weight loss of the carbonaceous part of the zeolite/carbon composite by oxidation in air in the range of 573−1073 K. [b] Determined using the data range $P/P_0 = 0.01-0.05$ from the N_2 isotherm at 77 K. [c] Total pore volume determined at $P/P_0 = 0.95$ from the N_2 isotherm at 77 K. [d] From the DR equation using the N_2 isotherm at 77 K. [e] $V_{meso} = V_t - V_{micro}$. [f] Measured by He pycnometry. [g] Calculated by the relation $\rho_{app} = 1/(V_t + 1/\rho_{skeletal})$.

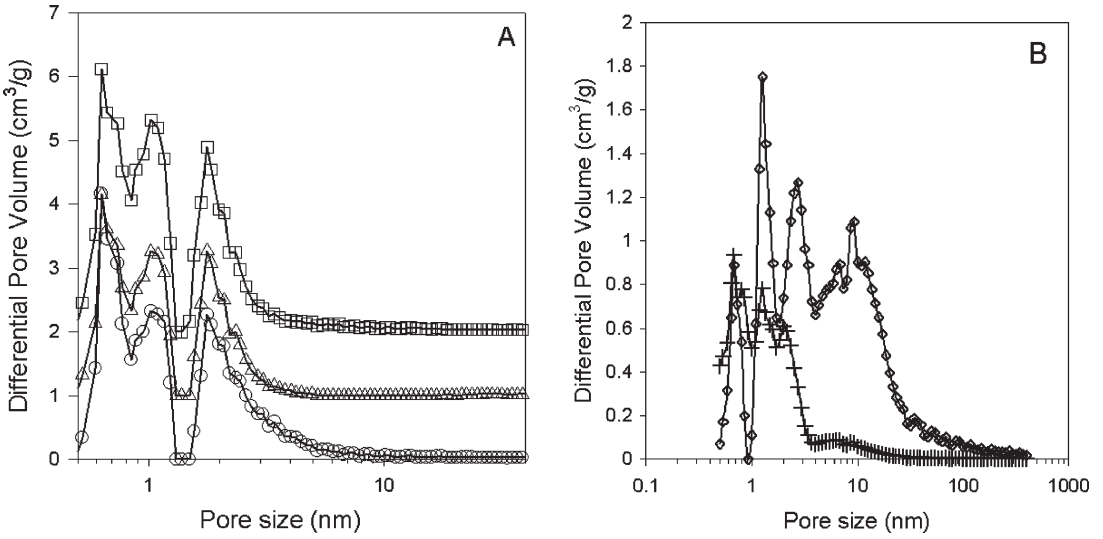

Figure 3. PSD curves determined by applying the DFT method to the N_2 adsorption isotherms (77 K) of (A) carbon replicas (○) Ac-873/973-4/1, (△) FA+Ac-923-5 (y axis + 1), and (□) FA+Ac-873/973-4/1 (y axis + 2) and (B) activated carbons (+) AC35 and (◇) BG-ENO.

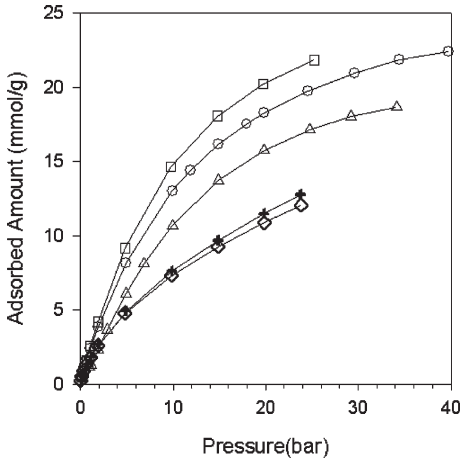

Figure 4. CO_2 adsorption isotherms at 298 K of the carbon replicas (△) FA+Ac-923-5, (○) Ac-873/973-4/1, and (□) FA+Ac-873/973-4/1 and activated carbons (+) AC35 and (◇) BG-ENO.

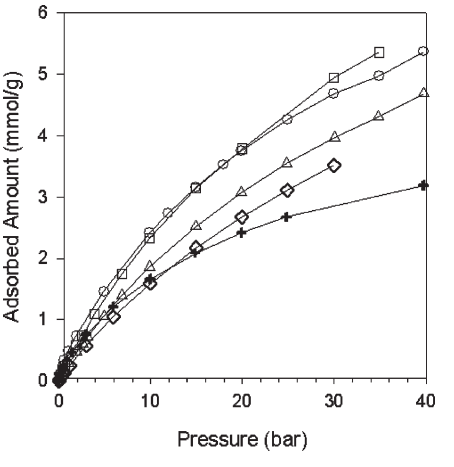

Figure 5. N_2 adsorption isotherms at 298 K of the carbon replicas (△) FA+Ac-923-5, (○) Ac-873/973-4/1, and (□) FA+Ac-873/973-4/1 and activated carbons (+) AC35 and (◇) BG-ENO.

ordered sample FA+Ac-923-5, always adsorb more than the two commercial activated carbon samples that were tested for comparison. The difference between the replicas and the conventional carbons is more pronounced for CO_2 and CH_4 than for N_2.

Table 2 compares the Langmuir fits of the CO_2, CH_4, and N_2 isotherms of the five samples. The Langmuir equation does not always allow us to represent the isotherm perfectly, but its parameters (q_s and b) are easy to interpret. We observe that AC35 systematically has the largest adsorption constant and the other samples have comparable values. The saturation capacity q_s of the samples follows roughly the order of pore volumes. The only exception is BG-ENO, which has moderate q_s values, despite its large

total pore volume. If the micropore volume is used instead of the total pore volume, the correlation with the q_S values becomes much better. This suggests that mesopores are not entirely filled in the pressure and temperature conditions used. To estimate whether CO_2 can adsorb in the mesopores under our experimental conditions, we have used the Dubinin−Radushkievich equation in combination with Stöckli's and Dubinin's relation between the adsorption energy E and the pore size d

$$\theta(d,P) = \exp\left[-\left(\frac{1}{-E_0(d)\beta}\right)^2\left(RT\ln\frac{P_0}{P}\right)^2\right] \quad (4)$$

$$E_0(d)\ (\mathrm{kJ/mol}) = \frac{10.8}{d\ (\mathrm{nm})} + 11.4 \text{ for } d = 0.35-1.3\ \mathrm{nm} \quad (5)$$

$$E_0(d)\ (\mathrm{kJ/mol}) = \frac{24}{d\ (\mathrm{nm})} \text{ for } d > 1.3\ \mathrm{nm} \quad (6)$$

where θ is the occupation of a pore of the size d, E_0 is the characteristic adsorption energy, which is related to the pore size via eqs 5 or 6, β is the affinity coefficient and has a value of 0.35 in the case of CO_2, and P_0 is the saturation vapor pressure of CO_2 at 298 K (P_0 = 64.1 bar). The function $\theta(P)$ for different pore sizes, which correspond to maxima in the PSD of BG-ENO (see Figure S2 in the Supporting Information), shows that pores width of d = 6 and 10 nm are only very partly occupied at a pressure of P = 20 bar. These pores represent almost 50% of the total pore volume of BG-ENO but do not contribute much to the adsorption capacity in the pressure range investigated.

The initial slopes of the isotherms are characterized by the product $K_{Henry} = q_s b$. The Henry constants of the two well-ordered carbon replicas are always the highest, followed by AC35 and FA+Ac-923-5. We can use the ratio of the Henry

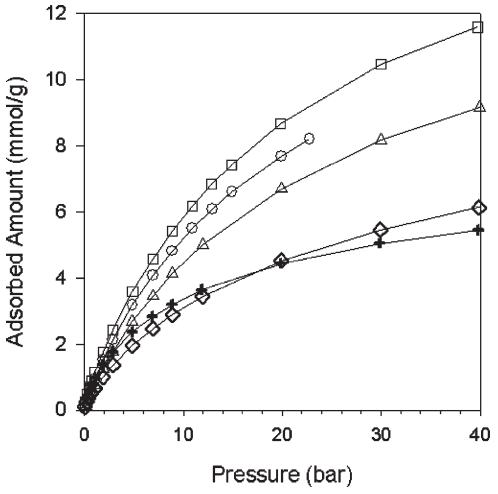

Figure 6. CH_4 adsorption isotherms at 298 K of the carbon replicas (△) FA+Ac-923-5, (○) Ac-873/973-4/1, and (□) FA+Ac-873/973-4/1 and activated carbons (+) AC35 and (◇) BG-ENO.

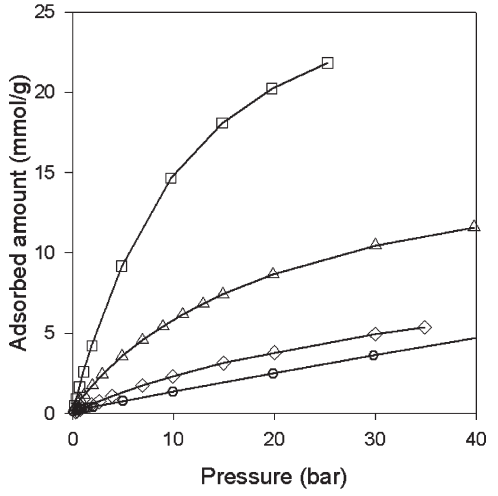

Figure 7. (□) CO_2, (△) CH_4, (◇) N_2, and (○) H_2 adsorption isotherms at 298 K of the carbon replica FA+Ac-873/973-4/1.

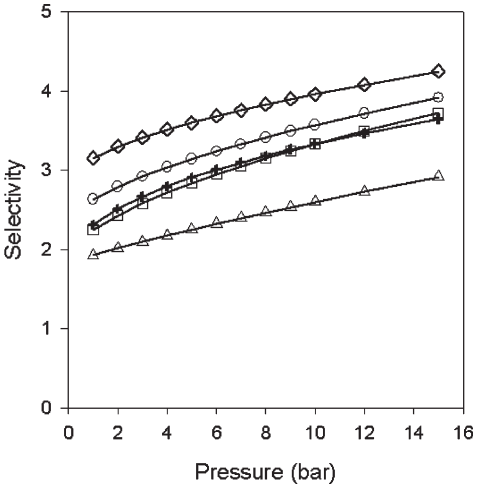

Figure 8. Evolution of the predicted selectivity of mixtures CO_2/CH_4 = 50:50 depending upon the pressure: (△) FA+Ac-923-5, (○) Ac-873/973-4/1, (□) FA+Ac-873/973-4/1, (+) AC35, and (◇) BG-ENO.

Table 2. Adsorbed Quantities at Saturation (q_s), Adsorption Constants (b), and Henry's Law Constants of the Carbon Replicas and Activated Carbons Obtained from the Langmuir Equation from CO_2, CH_4, and N_2 Isotherms at 298 K

	q_s (mol/kg)			constant b (bar^{-1})			Henry's law constant (mol kg^{-1} bar^{-1})			selectivity[a]	
	CO_2	CH_4	N_2	CO_2	CH_4	N_2	CO_2	CH_4	N_2	CO_2/CH_4	CO_2/N_2
Ac-873/973-4/1	29.8	14.2	8.6	0.080	0.059	0.039	2.37	0.83	0.34	2.85	6.96
FA+Ac-923-5	29.2	13.9	9.1	0.056	0.048	0.026	1.64	0.66	0.24	2.47	6.93
FA+Ac-873/973-4/1	34.1	16.6	10,9	0.073	0.052	0.027	2.50	0.87	0.30	2.88	8.38
AC35	10.9	6.4	5.0	0.166	0.118	0.044	1.81	0.76	0.22	2.39	8.14
BG-ENO	18.1	8.8	8.5	0.076	0.056	0.023	1.38	0.49	0.20	2.79	6.97

[a] Calculated from the ratio of the Henry constants.

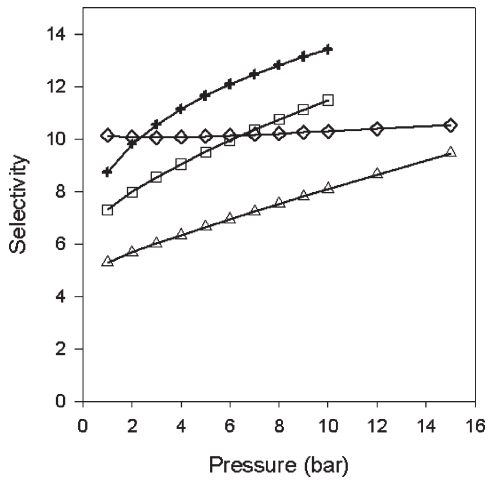

Figure 9. Evolution of the predicted selectivity of mixtures CO_2/N_2 = 50:50 depending upon the pressure: (△) FA+Ac-923-5, (□) FA+Ac-873/973-4/1, (+) AC35, and (◇) BG-ENO.

constants to calculate the CO_2/CH_4 and CO_2/N_2 selectivity at low pressures (see Figures 8 and 9). The CO_2/CH_4 and CO_2/N_2 selectivities are in the range of 2.5−2.9 and 6.9−8.4, respectively. Given the error margin of the determination of the Henry constants, the difference in selectivity between the samples is not significant. To obtain an estimate of the selectivity at higher pressures, the IAST was used.

At low pressures, the selectivity predicted by IAS tends to similar values as that obtained from the ratio of the Henry constants in Table 2. The small discrepancies between IAS and Table 2 arise from the difficulties to describe the isotherms perfectly by the Langmuir or Toth model. IAS predicts that the CO_2-CH_4 selectivity increases with pressure. This trend has also been found experimentally on activated carbon[21] and can be attributed to intermolecular CO_2-CO_2 interactions. Moreover, IAS classifies the selectivity of the five samples into three categories. The chemically activated carbon BG-ENO is the most selective material, and well-replicated carbon replicas have intermediate selectivity, whereas the carbon replica of lowest quality, FA+Ac-923-5, is the least selective material. The same trend is found when looking at the IAS predictions of the CO_2/N_2 selectivity, but here, activated carbon AC35 gives the best selectivity (Figure 9).

The observation that the low-quality replica has a lower selectivity than the high-quality replicas is surprising and requires a more detailed investigation of the relation between porosity and selectivity,[29] which is beyond the scope of the present paper.

For the best replica, i.e., for FA+Ac-873/973-4/1, we have also calculated the CO_2/H_2 and CH_4/H_2 selectivities. They are in the order of 17−18 for CO_2/H_2 and 6−10 for CH_4/H_2, respectively, with selectivity decreasing with pressure. These selectivities are somewhat lower than experimental results obtained on conventional activated carbons.[21]

Discussion

We first discuss how the adsorption isotherms of the five samples studied in this work are related to their textural properties and their surface chemistry. The adsorption of CO_2, CH_4, and N_2 on carbon materials depends upon at the same time the surface chemistry (defects, functional groups at the surface, etc.) and the textural properties. Differences in surface chemistry probably explain why the activated carbons BG-ENO and AC35 have the highest CO_2/CH_4 and CO_2/N_2 selectivities, respectively, as well as the high adsorption constant of AC35. Because of the influence of the surface chemistry, it is difficult to establish quantitative relationships between the porosity of the samples and the adsorption isotherms. There is, for example, no correlation between the surface area of the samples and the Henry constants of Table 2.

Table 3. Delta Loading of CO_2 Calculated for a Feed of 16% CO_2, 4.5% CH_4, 4.5% CO, and 75% H_2 at a Pressure of 22 bar, with Desorption at 1 bar and 298 K

	delta loading CO_2	
	mol/kg	mol/m^3
Ac-873/973-4/1	4.16	2370
FA+Ac-873/973-4/1	4.78	2340
AC35	2.14	1970
BG-ENO	2.22	1110

However, some qualitative relations between the textural properties (the PSDs) and the adsorption isotherms can be identified. We mentioned in the Results that the difference between the adsorption capacities of the five samples studied here is larger in the case of CO_2 and CH_4 than in the case of N_2. The difference between the CO_2 and CH_4 isotherms of the carbon replicas and the commercial activated carbon samples is accentuated at high pressures. At low pressures, the molecules adsorb preferentially in the narrowest pores, which have the strongest confinement effect. In the range of narrow micropores, which covers only the low-pressure portion (< 5 bar) of the CO_2 and CH_4 isotherms and a large portion of the N_2 isotherms, the carbon replicas do not have a higher adsorption capacity than the activated carbons (also compare to Figure S1 in the Supporting Information). Only when the large pore volume of the replica at a pore size of d = 1.1 nm starts to be filled, these samples clearly gain adsorption capacity compared to the activated carbons. The pressure at which this "transition" occurs appears to be between 2 and 5 bar for CO_2 and CH_4 and at much higher pressures for N_2 (which is the most volatile molecule of the three).

We have also compared our adsorption isotherms to data published by Himeno et al.[26] and Sheikh et al.,[27] who compared the adsorption of CO_2 and CH_4 on activated carbons covering a range of different textural properties and fabrication procedures. The adsorption capacities of the three carbon replicas reported in this work outperform the five samples studied in ref 26, including Maxsorb (see Table S3 in the Supporting Information). Maxsorb is an activated carbon with a very high surface area (3250 m^2/g) and a huge pore volume (1.8 cm^3/g).[28] Its pore size is distributed between 1 and 2 nm, with a maximum close to 1 nm. The textural properties of Maxsorb therefore appear quite close to our carbon replicas of zeolite NaY, but its porosity is not organized. The comparison to Maxsorb is therefore further evidence for the benefit of the nanocasting process. Moreover, the replicas have significantly higher apparent densities (0.5−0.7 g/cm^3) than Maxsorb (0.30 g/cm^3), whose adsorption capacity per volume is therefore almost a factor of 2 lower than one of our carbon replicas.

(26) Himeno, S.; Komatsu, T.; Fujita, S. *J. Chem. Eng. Data* **2005**, *50*, 369–376.
(27) Sheikh, N. A.; Hassan, M. M.; Loughlin, K. F. *Gas Sep. Purif.* **1996**, *10*, 161–168.
(28) Otowa, T.; Tanibata, R.; Itoh, M. *Gas Sep. Purif.* **1993**, *7*, 241–245.
(29) Cracknell, R. F.; Nicholson, D.; Tennison, S. R.; Bromhead, J. *Adsorption* **1996**, *2*, 193–203.

Finally, we turn toward our initial goal, which was to evaluate the performance of the carbon replica as adsorbents in H_2 PSAs. As mentioned in the Introduction, the main performance criterion is the cyclic adsorption capacity per adsorbent volume. The cyclic adsorption capacity is the difference between the adsorbed amount at the end of the adsorption step at high pressures and the adsorbed amount at the end of the desorption step at low pressures. Neglecting mass-transfer phenomena, the working capacity can be estimated from the co-adsorption equilibria. The amount adsorbed at high pressures q_{HP} is calculated for the pressure and composition of the feed. A typical molar composition of synthesis gas generated by methane steam reforming, after high-temperature water−gas shift and condensation of the excess water, is 16% CO_2, 4.5% CH_4, 4.5% CO, and 75% H_2. The total pressure is typically 22 bar, which means that the partial pressure of CO_2 is 3.5 bar and the partial pressures of CH_4 and CO are 1 bar. Then, q_{HP} (CO_2) is a function of p_{ads}, $y_{CO_2,feed}$, $y_{CH_4,feed}$, and $y_{CO,feed}$.

The adsorbent is then regenerated by a depressurization and a purge. During these steps, the more weakly adsorbed components CO and CH_4 desorb preferentially, which changes the molar fractions in the gas and adsorbed phases. To avoid calculations of the real concentration profiles, we made the simplifying assumption that the average gas-phase composition during desorption is close to composition of the adsorbed phase at adsorption pressure. The amount of CO_2 adsorbed at low pressures q_{LP} is therefore estimated considering the following parameters: p_{des}, $y_{CO_2} = x_{CO_2,ads}$, $y_{CH_4} = x_{CH_4,ads}$, and $y_{CO} = x_{CO,ads}$. The working capacity of CO_2 is then $q_{HP} - q_{LP}$.

The co-adsorption equilibria were calculated from the single-component adsorption isotherms via IAST. We did not dispose of the isotherms of CO for all of the samples tested in this work, but it is well-known that the adsorption properties of CO and N_2 on activated carbons are very similar.[30] We therefore substituted the isotherm of CO by N_2. Table 3 shows the delta loadings that were calculated by this method. The carbon replicas clearly outperform the activated carbon materials in terms of the delta loading per mass. The difference to AC35 diminishes when the loading per volume is compared because of the high apparent density of AC35. We stress, however, that the real apparent density of AC35 is much lower than the value calculated in Table 1 (0.67 versus 0.92 g/cm^3), because of the large fraction of macropores in the pellets.

Conclusions

The adsorption and separation properties of zeolite Y carbon replicas were investigated in the framework of H_2 purification. These materials were obtained using FA and Ac as carbon precursors. The high pore volume in combination with the PSD centered at 1.0 nm gives the materials a very high adsorption capacity in the intermediate-pressure range (5−30 bar). They outperform micro- and mesoporous activated carbons because of the higher micropore volume and the much narrower PSD in the super-micropore range, respectively. Their adsorption capacity is also superior to Maxsorb, an activated carbon with similar textural properties but with non-organized porosity. The adsorption capacities of the carbon replicas are correlated to the quality of replication of the zeolite Y mold, which highlights the importance of producing materials with a high degree of ordering and a well-defined PSD.

The separation selectivities of the carbon replicas were estimated from the ratio of the Henry constants as well as from IAST. They are in the same range as those of the commercial activated carbons (the small observed differences require a more detail investigation of the surface chemistry of the materials, which is beyond the scope of this paper). The fact that the carbon replicas have similar selectivities as commercial activated carbons but higher adsorption capacities (per mass and per volume) dramatically increases their working capacity compared to conventional activated carbons. Therefore, these materials are very attractive adsorbents for H_2 purification by PSA. In this context, the use of a more appropriate zeolite template to decrease the nano-ordered pore size and/or the addition of peculiar surface chemical functionalities merit consideration for future studies to enhance the selectivity of these microporous carbon replicas while preserving their outstanding high adsorption capacities.

Whether the carbon replica will find a place as adsorbents in industrial processes will, however, also depend upon economic considerations. The current multi-step preparation procedure makes these materials a lot more expensive than conventional activated carbon materials. Therefore, a further challenge for future research is to find a simpler, less onerous, and less expensive synthesis route.

Acknowledgment. We acknowledge Jean-Pierre Courcy for carrying out part of the adsorption measurements and Elsa Jolimaître for many stimulating discussions and helpful comments on the manuscript (both IFP).

Supporting Information Available: DFT pore size cumulative volume graph of carbon replicas (Figure S1), constructed composite Dubinin−Radushkievitch isotherms of BG-ENO for CO_2 at 298 K for various values of pore size (Figure S2), and Henry's law constants of the activated carbons from ref 26 at 300 K (Table S3). This material is available free of charge via the Internet at http://pubs.acs.org.

(30) Agarwal, R. K.; Schwarz, J. A. *Carbon* **1988**, *26*, 873–887.